

Fermi-surface origin of skyrmion lattices in centrosymmetric rare-earth intermetallics

Juba Bouaziz,^{1,2,*} Eduardo Menvive-Tapia,^{1,3} Stefan Blügel,¹ and Julie B. Staunton²

¹*Peter Grünberg Institut and Institute for Advanced Simulation,
Forschungszentrum Jülich & JARA, D-52425 Jülich, Germany*

²*Department of Physics, University of Warwick, Coventry CV4 7AL, United Kingdom*

³*Department of Computational Materials Design,
Max-Planck-Institut für Eisenforschung, 40237 Düsseldorf, Germany*

(Dated: April 5, 2022)

We show from first-principles that barrel-shaped structures within the Fermi surface of the centrosymmetric intermetallic compounds GdRu₂Si₂ and Gd₂PdSi₃ give rise to Fermi surface nesting, which determines the strength and sign of quasi-two-dimensional Ruderman-Kittel-Kasuya-Yosida pairwise exchange interactions between the Gd moments. This is the principal mechanism leading to their helical single- q spin-spiral ground states, providing transition temperatures and magnetic periods in good agreement with experiment. Using atomistic spin-dynamic simulations, we draw a direct line between the subtleties of the three-dimensional Fermi surface topology and the stabilization of a square skyrmion lattice in GdRu₂Si₂ at applied magnetic fields as observed in experiment.

Magnetic skyrmions have been under intense scrutiny over the last decade, mainly owing to their intriguing topological and transport properties [1], and prospect as entities for ultra-low power information storage and processing devices [2, 3]. Hexagonal skyrmion crystals (SkX) and single skyrmions are prevalent in non-centrosymmetric materials where they emerge from the competition between ferromagnetic exchange and the Dzyaloshinskii-Moriya interaction (DMI) in the presence of small applied magnetic fields [2, 4]. The small energy scale of the relativistic DMI gives rise to skyrmions with typical sizes of tenths of nanometers or more. A path to still smaller skyrmions is provided by the replacement of the DMI by much larger antiferromagnetic exchange interactions competing with ferromagnetic ones on equal footing. A control of skyrmion formation by small applied fields is, therefore, not trivial [5].

More flexibility, which does not rely on DMI, can be obtained by exploiting intrinsically competing exchange interactions, such as Ruderman-Kittel-Kasuya-Yosida (RKKY) interactions, prevalent in centrosymmetric rare-earth intermetallics [6, 7]. Here the interaction between a pair of *e.g.* Gd atoms oscillates between being ferro- or antiferromagnetic depending on the magnitude of the position vector, $\mathbf{R}_1 - \mathbf{R}_2$, connecting the two atoms and its orientation within the lattice. The mechanism and strength is fundamentally linked to the topology and nesting features of the Fermi surface (FS) [6, 8], the symmetry of the crystal, and the conduction electrons that own the FS. Based on a model for conduction electrons described by a nearly isotropic two-dimensional (2D) electron gas, Wang *et al.* [9] indeed pointed out the possibility of stabilizing a hexagonal skyrmion crystal (SkX) phase by the RKKY interaction.

Recently, skyrmion crystals with small lattice constants were experimentally uncovered for two different centrosymmetric ternary Gd-4*d*-transition-metal intermetallic compounds: Gd₂PdSi₃, formed by stacked

hexagonal Gd layers, exhibiting a hexagonal SkX with a lattice constant of ~ 2.5 nm [10], and GdRu₂Si₂, where 2D sheets of Gd atoms arranged on a square lattice separated by layers of Ru and Si atoms exhibit a square lattice of skyrmions, a so-called double- q SkX, with an even smaller lattice constant of 1.9 nm [11]. The SkX phases with their small lattice constants display many interesting properties, *e.g.* a giant topological Hall effect [10, 12], a large topological Nernst [13], and a planar Hall effect [14].

In contrast to the SkX formation suggested by the RKKY model of Wang *et al.* [9], a recent theoretical in-depth analysis fundamentally rejected the RKKY mechanism for both compounds and proposed an inter-orbital Gd *d-f* frustration as direct exchange mechanism between Gd atoms [15].

In this letter, we demonstrate fully from first-principles, that the RKKY paradigm is the central mechanism in GdRu₂Si₂ and Gd₂PdSi₃ giving rise to a nanometric single- q spiral state. This spiral forms within the Gd planes, weakly ferromagnetically coupled along the *c*-direction, and transforms to a SkX under an applied magnetic field. We show how the formation of a three-dimensional (3D) barrel-shaped FS topology around the Γ point and its subsequent nesting directly coincides with the large formation energy and the wave vector \mathbf{q} of the spin spiral. The 3D itinerant valence electron glue of primarily 4*d* Ru or Pd electrons hybridizing with the 5*d* electrons of Gd mediates the magnetic interactions between the Gd atoms. We calculate the transition temperatures, finding a good quantitative agreement with experiments [10, 11].

We go on to investigate the effect of an external magnetic field, B , applied to GdRu₂Si₂. We show that the lowest energy state at intermediate magnetic fields corresponds to a $2q$, square SkX that arises directly from the combination of crystal symmetry-dependent frustrated RKKY interactions with a simple uniaxial magnetocryst-

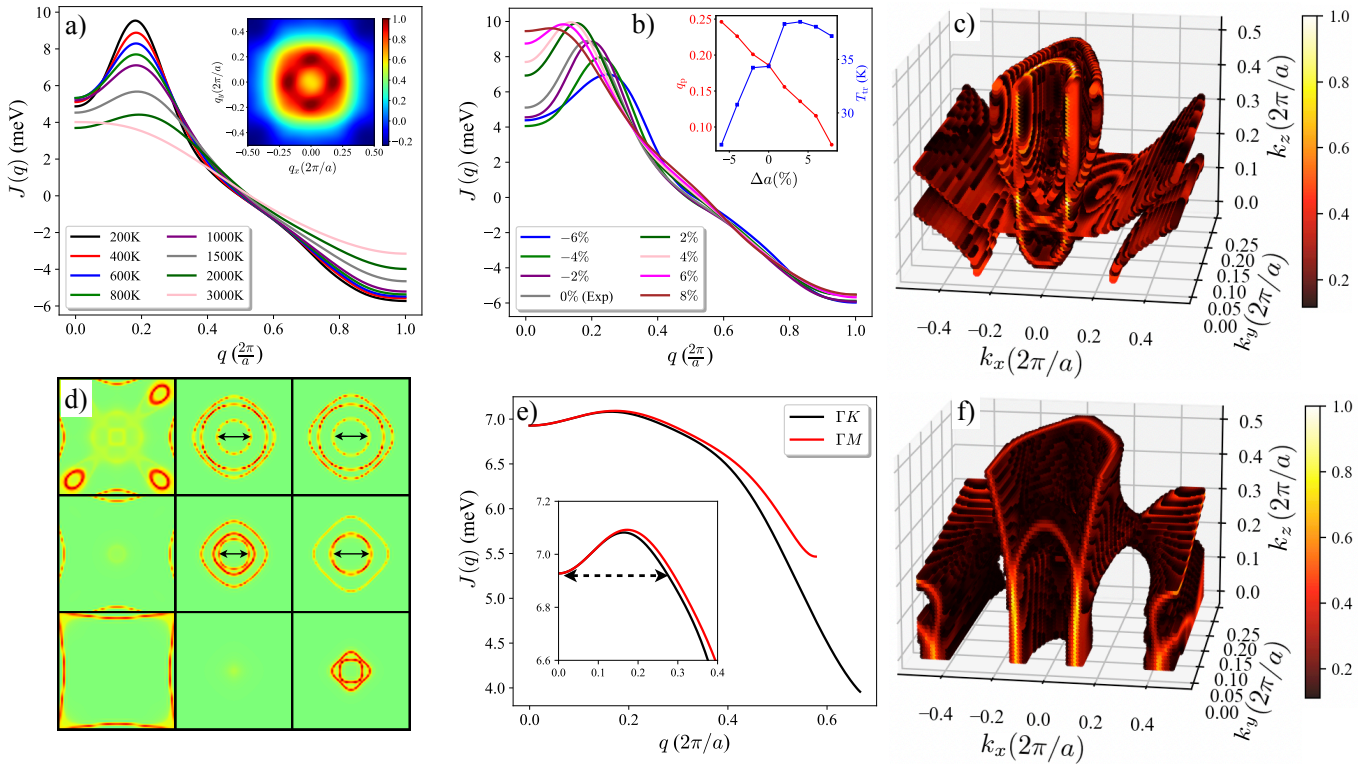


FIG. 1. a) Fourier transform, $J(\mathbf{q})$, of the magnetic interactions for different electronic temperatures at the experimental lattice parameter $a_{\text{exp}} = 4.162 \text{ \AA}$ of GdRu_2Si_2 against the wave vector \mathbf{q} along the [100] direction. The inset shows a colormap encoding the size of $J(\mathbf{q})$ within the $q_z = 0$ plane. b) $J(\mathbf{q})$ of GdRu_2Si_2 for different lattice compressions and expansions. c,f) Fermi surfaces of GdRu_2Si_2 and Gd_2PdSi_3 , respectively, where the color indicates the intensity of the spectral weight $A_B(\mathbf{q}, E)/\max_{\mathbf{q}, E} A_B(\mathbf{q}, E)$. d) Cuts of Fermi surface of GdRu_2Si_2 at $k_z \in \{0, 0.3, 0.5\} \frac{2\pi}{a}$, from left to right, with $a = a_{\text{exp}} - 6\%$ (upper panels), $a = a_{\text{exp}}$ (middle panels), and $a = a_{\text{exp}} + 8\%$ (lower panels). e) $J(\mathbf{q})$ of Gd_2PdSi_3 along the ΓK and ΓM directions.

talline anisotropy and a magnetic field perpendicular to the helical axis. While four-spin interactions can favor the stability of multiple- q states and square SkX, as explained in Refs. [11, 16, 17], our results demonstrate that multisite interactions are not necessary to produce the square SkX in GdRu_2Si_2 . We also show that the SkX phase exhibits a strong magneto-elastic coupling.

We employ the Green function-based formulation of density functional theory using the scalar relativistic, all-electron full-potential Korringa-Kohn-Rostoker (KKR) method [18, 19]. The exchange-correlation energy is treated in the generalized gradient approximation (GGA) [20]. The magnetic pair interactions, $\{J_{ij}\}$, are computed using the infinitesimal rotation method in the ferromagnetic state [21–23].

RKKY mechanism and Fermi surface nesting in GdRu_2Si_2 and Gd_2PdSi_3 – Taking the lattice Fourier transform of $\{J_{ij}\}$ gives the Gd-Gd interaction in wave vector (momentum) space, $J(\mathbf{q})$ [24] (see Supplemental Material for details [25]). The highest value of $J(\mathbf{q})$ determines the Néel temperature and the wave vector \mathbf{q}_p of the spiroidal magnetic single- q state of lowest energy, while the energy difference, $J(\mathbf{q}_p) - J(\mathbf{0})$, describes its

stability with respect to the ferromagnetic one. Fig. 1(a) shows $J(\mathbf{q})$ along the [100] direction for GdRu_2Si_2 evaluated using the experimental lattice parameter. It features a typical paramagnetic spin susceptibility of a metal with a FM ground state augmented by a sharp, significant finite- q peak at $q_p = 0.19 \frac{2\pi}{a}$. This is consistent with the low temperature stabilization of an incommensurate helimagnetic state, in very good agreement with the experiment, $q_p^{\text{exp}} = 0.22 \frac{2\pi}{a}$ [11]. At low levels of thermally-induced single electron-hole excitations across the FS (e.g. electronic temperature of 200 K), $J(\mathbf{q}_p) = 9.5 \text{ meV}$, nearly twice the size of $J(\mathbf{0}) = 4.9 \text{ meV}$. This peak is consistent to the long-range magnetic interactions that extend somewhat further than three lattice constants, in accordance with an RKKY picture [26]. For example, if we only consider shorter interactions (below $3a$), we observe that $\mathbf{q}_p = \mathbf{0}$, and so a ferromagnetic state stabilizes instead. $J(\mathbf{q})$ can be conveniently analysed in terms of a Fermi sea contribution to the 3D bulk magnetic susceptibility, $J_{3D}(\mathbf{q})$, and the FS specific contribution to the RKKY interaction, $J_{\text{FS}}(\mathbf{q})$, $J(\mathbf{q}) = J_{3D}(\mathbf{q}) + J_{\text{FS}}(\mathbf{q})$. To distinguish J_{3D} from J_{FS} and provide further evidence for this RKKY mechanism with its fundamental link to the

FS, the effect of the electronic temperature T prescribed by the Fermi-Dirac distribution for the single electron-hole excitations is investigated. In Fig. 1(a), we demonstrate how the peak vanishes when T increases, which shows how the stabilization of the spiral state is strongly tied to the itinerant valence electronic structure. We also highlight that $J(\mathbf{q})$ peaks along all directions within the $\mathbf{q} = (q_x, q_y, 0)$ plane with roughly the same size of the wave vector q_p . The peak height is modulated and thus the strength of the RKKY interaction varies in accordance with the C_{4v} symmetry of the crystal lattice. This is shown in the inset of Fig. 1(a), which is a color map for the value of $J(\mathbf{q})$ in the $q_z = 0$ plane. No peak is observed in the out-of-plane directions.

Close scrutiny of the FS reveals how its topology is connected to the emergence of \mathbf{q}_p and the size of $J(\mathbf{q}_p)$. Fig. 1(c,f) shows the 3D FS of GdRu₂Si₂ as well as of Gd₂PdSi₃, where the color indicates the spectral weight [27]. These calculations are suitably performed in the paramagnetic state, which we describe by fully disordered local moments (DLM) averaged using the coherent potential approximation [28–30]. We have found in both materials the presence of barrel-shaped nested sheets with a large spectral weight located around the Γ point. Their correlation with \mathbf{q}_p in GdRu₂Si₂ can be seen by examining FS cuts at $k_z \in \{0, 0.3, 0.5\} \frac{2\pi}{a}$, see Fig. 1(d). For the experimental lattice parameter (middle panels), we observe that the magnitude of the wave vector of the magnetic spiral, \mathbf{q}_p , matches the nesting vector \mathbf{k}_N , *i.e.* the Bloch wave vector spanning the barrel-like nesting in the (k_x, k_y) plane and showing C_{4v} symmetry of the crystal. The length of \mathbf{k}_N , indicated by a black arrow (\leftrightarrow), increases (reduces/disappears) when the in-plane lattice parameter a decreases (increases), keeping the out-of-plane lattice constant fixed, as shown in the upper (lower) panels. We observe that this directly correlates with the size of \mathbf{q}_p plotted in Fig. 1(b) for different values of a . In other words, the barrel collapses when the peak vanishes [see Fig. 1(d)].

The Fourier transform of the magnetic interactions described by an RKKY mechanism is directly proportional to the paramagnetic susceptibility of the valence electrons, dominated by the convolution of the Bloch spectral functions, $A_B(\mathbf{k}, E)$, at the Fermi energy, E_F , at low temperature

$$J_{\text{FS}}(\mathbf{q}) \approx \int_{\text{BZ}} d\mathbf{k} A_B(\mathbf{k}, E_F) A_B(\mathbf{k} + \mathbf{q}, E_F). \quad (1)$$

$J_{\text{FS}}(\mathbf{q})$, therefore, should present a peak at \mathbf{q}_p when the FS contains nesting features [8]. Making an ansatz of a 2D electron dispersion $E(k_x, k_y)$, Wang *et al.* [9] showed the presence of a small nesting induced peak of $J(\mathbf{q})$. However, if the nesting condition holds during the integration along the third dimension k_z in the 3D barrel-shaped FS as shown in Fig. 1(c,d,f), the peak of $J_{\text{FS}}(\mathbf{q}_p) \approx J(\mathbf{q}_p) - J(\mathbf{0}) \propto H$ scales with the height H

of the barrel.

Also for Gd₂PdSi₃ a similar pipe-like shape in the FS forms with a nesting vector that is very close to $q_p = 0.17 \frac{2\pi}{a}$ (in the ΓM direction) as shown in Fig. 1(e,f). This value is also in good agreement with experiment, $q_p^{\text{exp}} = 0.14 \frac{2\pi}{a}$ [10, 31]. The set of $\{J_{ij}\}$, and $J(\mathbf{q})$, inherit the hexagonal symmetry of this compound such that the \mathbf{q} -vector of the spiral wave follows the high-symmetry direction of the Gd lattice. The strongest hexagonal warping is present for a nesting vector $k_N \approx q_p$, from which the finite peak originates in $J(\mathbf{q})$. The size of the nesting vector, $k_N(k_z)$ depends on k_z , as shown in Fig. 1(f). The largest length is $k_N \approx 0.4 \frac{2\pi}{a}$ directly relates to the width of the peak of $J(\mathbf{q})$ as indicated by a black dashed line in Fig. 1(e).

Transition temperature – A mean-field estimation of the Néel transition temperature from the paramagnetic state is provided by $T_N = \frac{J(\mathbf{q}_p)}{3k_B}$, k_B being the Boltzmann constant. For the corresponding experimental lattice parameters we have obtained $T_N = 34$ K, a spiral period of ($\lambda = 2\pi/q_p$) $\lambda = 2.19$ nm and a magnetic moment of $M_{\text{Gd}} = 7.048 \mu_B$ for GdRu₂Si₂, and $T_N = 27$ K, $M_{\text{Gd}} = 7.057 \mu_B$, and $\lambda = 4.77$ nm for Gd₂PdSi₃. The computed transition temperatures are in excellent agreement with experiment, $T_N^{\text{exp}} = 46$ K (GdRu₂Si₂) and $T_N^{\text{exp}} = 20$ K (Gd₂PdSi₃), and the theoretical spiral periods correctly lie within the experimental nanometer scale, $\lambda^{\text{exp}} = 1.90$ nm (GdRu₂Si₂) [11] and $\lambda^{\text{exp}} = 5.82$ nm (Gd₂PdSi₃) [10].

Magneto-elastic coupling – In the inset of Fig. 1(b), we show q_p and the transition temperature of GdRu₂Si₂ as functions of the in-plane lattice parameter a while keeping c fixed. A lattice compression of -6.0% enhances q_p from $0.19 \frac{2\pi}{a}$ to $0.25 \frac{2\pi}{a}$ whereas an expansion progressively reduces the energy difference $J(\mathbf{q}_p) - J(\mathbf{0})$ and the wave vector q_p to reach almost zero at 8% . In contrast the Néel temperature, T_N , increases (decreases) for lattice expansion (contraction) and ranges over $24 - 38$ K.

Skyrmion crystal – We now turn our attention to the stabilization of a SkX phase in GdRu₂Si₂ upon application of a magnetic field. Experimentally, it has been reported that the wave vector \mathbf{q}_p is normal to the plane of the helimagnetic state at zero magnetic field [11, 32]. This magnetic state is in line with an easy c -axis magnetic anisotropy as reported in Ref. [33]. The formation of a $2q$ -SkX state is found when an external magnetic field is applied along the c -axis, *i.e.* parallel to the magnetization plane of the helimagnetic state. As the applied B -field is increased, the helix is distorted until the field reaches $\simeq 2$ T, at which a phase transition to the SkX state occurs. This SkX state remains stable for temperatures up to $\simeq 20$ K. When the field is increased further, initially a cycloid magnetic phase emerges, which then changes to a saturated ferromagnetic state [11].

A natural path to identify the magnetic phases present in GdRu₂Si₂ is to analyse a micromagnetic energy func-

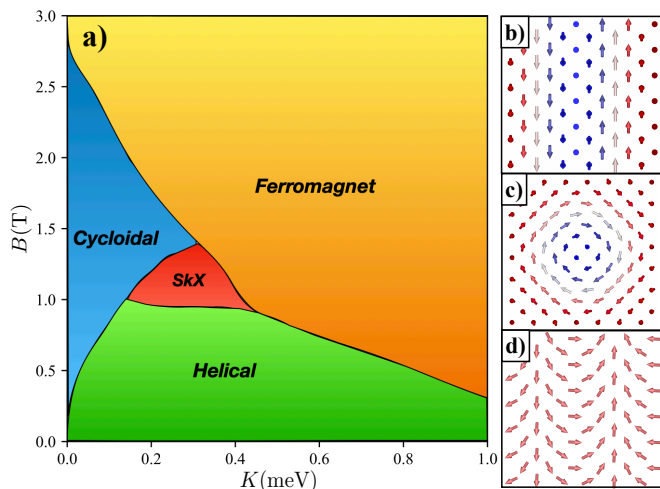


FIG. 2. a) GdRu₂Si₂ magnetic phase diagram exhibiting four different phases in the (K, B) parameter space. K is magneto-crystalline anisotropy and B is the magnetic field. (b-d) Representative magnetic textures (color indicates the m_z component, blue: $m_z = -1$, red $m_z = 1$) described by the Gd moments at lattice sites bct crystal structure corresponding to: (b) helical state for $(K, B) = (0.2, 0.6)$, (c) SkX for $(K, B) = (0.2, 1.0)$ and (d) cycloidal for $(K, B) = (0.1, 1.0)$.

tional. By fitting $J(q)$ for small q , as $J(q) \simeq \mathcal{A}q^2 + \mathcal{B}q^4 + \mathcal{C}q_x^2q_y^2$ (\mathcal{A} to \mathcal{C} being constants) and then taking the continuum limit, we identify higher-power gradient terms such as $q^4 \leftrightarrow (\nabla^2 \mathbf{m})^2$ of the magnetization density \mathbf{m} as the stabilization mechanism of a SkX [34, 35]. However, to cover the short magnetic wavelengths, even higher powers of q would be required in the fit. Therefore, to tackle this complexity more effectively, we adopt an atomistic description where we use directly the magnetic interactions which we have computed from first-principles (see Fig. 1). We use the internal energy:

$$\mathcal{E}_m = -\frac{1}{2} \sum_{ij} J_{ij} \mathbf{m}_i \cdot \mathbf{m}_j - K \sum_i (\mathbf{m}_i \cdot \mathbf{e}_z)^2 - \mathbf{B} \cdot \sum_i \mathbf{m}_i, \quad (2)$$

where \mathbf{m}_i is the direction of the magnetic moment at Gd-site i , K is a magneto-crystalline anisotropy constant and \mathbf{B} is the external magnetic field applied along the c -axis. The minimization of \mathcal{E}_m is achieved by solving the Landau-Lifshitz-Gilbert equation as implemented in the Spirit code [36] (details on the construction of the phase diagram are given in [25]).

The (K, B) magnetic phase diagram is presented in Fig. 2(a). It displays four distinct magnetic phases: cycloidal, helical, SkX and a field-saturated ferromagnetic state. The magnetic textures of the first three phases are depicted in Figs. 2(b-d). Ignoring the demagnetization field, due to the absence of DMI in centrosymmetric compounds, left- and right-handed single- q helical or cycloidal states as well as lattices of Néel- or

Bloch-type or anti-skyrmions (ASkX), have the same energy [37]. Experimentally, the magnetic structures can be distinguished measuring various magnetic structure factors [25].

For the case $(K, B) = (0, 0)$, the cycloidal and helical phases are degenerate. For relatively low K and moderate B -field, the cycloidal phase is favored. At the line $(0, B)$ we find the saturation field of about 3T that corresponds to the unwinding energy of the cycloidal state into the field-saturated ferromagnetic one, $J(\mathbf{q}_p) - J(0)$. When the value of magnetic anisotropy is increased, the cycloidal phase becomes less stable and the phase boundaries of the ferromagnetic and helical phase move towards the cycloidal phase. In the window $0.95 \leq B \leq 1.4$ T and $0.15 \leq K \leq 0.45$ meV, a pocket with a 2D skyrmion lattice phase of C_{4v} square symmetry emerges, which is attributed to the four-fold anisotropy in $J(\mathbf{q})$ [Fig. 2(c)]. The critical magnetic field necessary to stabilize this skyrmion lattice phase is approximately half of the experimental value [11]. The difference is energetically small and could be due, e.g., to the precise choice of lattice parameters or small higher order interactions.

We calculate the approximate skyrmion lattice constant to be $A_{\text{Sk}} \simeq 2.5$ nm, which is close to the wavelength of $\lambda = 2.1$ nm we found for the $1q$ helical state in this compound. Besides the SkX phase we also found single skyrmions as meta-stable particles in the ferromagnetic phase close to the phase boundary to the cycloidal and SkX phases analogous to the discussion in Ref. [38].

The presence of a strong magneto-elastic coupling in GdRu₂Si₂ (see Fig. 1b) is also reflected in the behavior of the SkX phase under pressure. To illustrate this, we fix $\mathcal{K} = 0.3$ meV and use the J_{ij} parameters obtained above for a 4% (6%) compression (expansion). For 4% compression, the most stable state is cycloidal for magnetic fields up to 4 T, while for 6% expansion the system collapses towards a saturated ferromagnetic state. Thus, we conclude that the SkX pocket is strongly dependent on the in-plane interatomic spacing. This finding is supported by experiments [39] on Gd₂PdSi₃, for which an expansion of the SkX phase was found upon uniaxial pressure.

Our materials specific first-principles results are in accord with the theoretical model of Wang *et al.* [9] based on a 2D electron gas. Both approaches put forward a RKKY-type interaction as the principal mechanism underlying the magnetism of the centrosymmetric materials investigated. Our results are quantitatively at odds with the ab-initio results reported by Nomoto *et al.* [15] and hence have a different interpretation. It is apparent that the subtle long-ranged interactions of oscillatory sign and small strengths in these compounds together with the small spin-polarization of the d orbitals relative to the large spin-moments associated with the Gd atoms requires a very careful assessment of all the technical or conceptual approximations which are used in their modelling.

Conclusion — Using GdRu_2Si_2 and Gd_2PdSi_3 as examples of intermetallic rare-earth compounds, we have demonstrated from first-principles that their long-range intrinsic RKKY interaction is able to generate single- q magnetic spiral phases that can form skyrmion lattices with small nanometric lattice constants when laboratory magnetic fields are applied. Single skyrmions have been found in the ferromagnetic phase near the phase boundaries to the cycloidal and skyrmion lattice. Our calculations directly link important skyrmion design parameters, such as the size, the symmetry, the Néel temperature or the applied magnetic field required to form skyrmion lattices or single skyrmions, to nesting conditions of the three-dimensional barrel-shaped Fermi surface. These can be modified and optimized in various ways, *e.g.* through the strong dependence on elastic deformations.

The frustrated exchange introduced by the RKKY interaction opens a new vista for the stabilization of small magnetic skyrmions and skyrmion lattices in centrosymmetric compounds. Considering that GdRu_2Si_2 and Gd_2PdSi_3 belong to two huge families of intermetallic compounds, there are many possibilities for material optimization. Both the intermixing or substitution of Gd with other rare earth ions either altering the lattice parameters or increasing the crystal field effects might reduce the necessary laboratory B -fields. Substituting $3d$ -atoms for the $4d$ -ones holds the prospect of greatly raising the transition temperature and realizing room-temperature skyrmions [40]. Indeed, from sources such as [41], we can identify 225 candidates belonging to thirteen centrosymmetric families of ternary rare-earth intermetallics with propensity for antiferromagnetic order and potential to host non-trivial spin textures [25]. Finally three-dimensional Fermi surface nesting can lead to three-dimensional modulated magnetization textures and thus a path to magnetic hopfions [34].

We thank Nikolai Kiselev, Phivos Mavropoulos, Markus Hoffmann and Moritz Sallermann for fruitful discussions. S.B. gratefully acknowledges financial support from the European Research Council (ERC) under the European Union’s Horizon 2020 research and innovation program (Grant No. 856538, project “3D MAGiC”), from Deutsche Forschungsgemeinschaft (DFG) through SPP 2137 “Skyrmionics” (Project BL 444/16) and the Collaborative Research Centers SFB 1238 (Project C01), respectively. J.B.S. acknowledges support from UK EPSRC Grant No. EP/M028941/1. J.B. and S.B. gratefully acknowledge the computing time granted by the JARA-CSD and VSR Resource Allocation Board provided on the supercomputers CLAIX at RWTH Aachen University and JURECA at Supercomputer Centre Jülich under grant nos. jara0219, jara3dmagic.

* j.bouaziz@fz-juelich.de

- [1] A. Neubauer, C. Pfleiderer, B. Binz, A. Rosch, R. Ritz, P. G. Niklowitz, and P. Böni, “Topological Hall Effect in the A Phase of MnSi ,” *Phys. Rev. Lett.* **102**, 186602 (2009).
- [2] N. Nagaosa and Y. Tokura, “Topological properties and dynamics of magnetic skyrmions,” *Nature nanotechnology* **8**, 899–911 (2013).
- [3] A. Fert, V. Cros, and Joao Sampaio, “Skyrmions on the track,” *Nature nanotechnology* **8**, 152–156 (2013).
- [4] U. K. Roessler, A.N. Bogdanov, and C. Pfleiderer, “Spontaneous skyrmion ground states in magnetic metals,” *Nature* **442**, 797–801 (2006).
- [5] Ashis Kumar Nandy, Nikolai S. Kiselev, and Stefan Blügel, “Interlayer exchange coupling: A general scheme turning chiral magnets into magnetic multilayers carrying atomic-scale skyrmions,” *Phys. Rev. Lett.* **116**, 177202 (2016).
- [6] I. D. Hughes, M. Däne, A. Ernst, W. Hergert, M. Lüders, J. Poulter, J. B. Staunton, A. Svane, Z. Szotek, and W. M. Temmerman, “Lanthanide contraction and magnetism in the heavy rare earth elements,” *Nature* **446**, 650–653 (2007).
- [7] E. Mendive-Tapia and J. B. Staunton, “Theory of magnetic ordering in the heavy rare earths: Ab initio electronic origin of pair- and four-spin interactions,” *Phys. Rev. Lett.* **118**, 197202 (2017).
- [8] J. Jensen and Allan R. Mackintosh, *Rare earth magnetism: structures and excitations* (Clarendon Oxford, 1991).
- [9] Z. Wang, Y. Su, S. Lin, and C. D. Batista, “Skyrmion Crystal from RKKY Interaction Mediated by 2D Electron Gas,” *Phys. Rev. Lett.* **124**, 207201 (2020).
- [10] T. Kurumaji, T. Nakajima, M. Hirschberger, A. Kikkawa, Y. Yamasaki, H. Sagayama, H. Nakao, Y. Taguchi, T. Arima, and Y. Tokura, “Skyrmion lattice with a giant topological hall effect in a frustrated triangular-lattice magnet,” *Science* **365**, 914–918 (2019).
- [11] N. D. Khanh, T. Nakajima, X. Yu, S. Gao, K. Shibata, M. Hirschberger, Y. Yamasaki, H. Sagayama, H. Nakao, L. Peng, *et al.*, “Nanometric square skyrmion lattice in a centrosymmetric tetragonal magnet,” *Nature Nanotechnology* **15**, 444–449 (2020).
- [12] J. Bouaziz, H. Ishida, S. Lounis, and S. Blügel, “Transverse transport in two-dimensional relativistic systems with nontrivial spin textures,” *Phys. Rev. Lett.* **126**, 147203 (2021).
- [13] M. Hirschberger, L. Spitz, T. Nomoto, T. Kurumaji, S. Gao, J. Masell, T. Nakajima, A. Kikkawa, Y. Yamasaki, H. Sagayama, H. Nakao, Y. Taguchi, R. Arita, T. Arima, and Y. Tokura, “Topological nernst effect of the two-dimensional skyrmion lattice,” *Phys. Rev. Lett.* **125**, 076602 (2020).
- [14] M. Hirschberger, T. Nakajima, M. Kriener, T. Kurumaji, L. Spitz, S. Gao, A. Kikkawa, Y. Yamasaki, H. Sagayama, H. Nakao, S. Ohira-Kawamura, Y. Taguchi, T. Arima, and Y. Tokura, “High-field depinned phase and planar Hall effect in the skyrmion host Gd_2PdSi_3 ,” *Phys. Rev. B* **101**, 220401 (2020).
- [15] T. Nomoto, T. Koretsune, and R. Arita, “Formation Mechanism of the Helical Q Structure in Gd-Based

- Skyrmion Materials,” *Phys. Rev. Lett.* **125**, 117204 (2020).
- [16] Ph. Kurz, G. Bihlmayer, K. Hirai, and S. Blügel, “Three-dimensional spin structure on a two-dimensional lattice: Mn/cu(111),” *Phys. Rev. Lett.* **86**, 1106–1109 (2001).
- [17] Stefan Heinze, Kirsten Von Bergmann, Matthias Menzel, Jens Brede, André Kubetzka, Roland Wiesendanger, Gustav Bihlmayer, and Stefan Blügel, “Spontaneous atomic-scale magnetic skyrmion lattice in two dimensions,” *Nat. Phys.* **7**, 713 (2011).
- [18] N. Papanikolaou, R. Zeller, and P. H. Dederichs, “Conceptual improvements of the KKR method,” *Journal of Physics: Condensed Matter* **14**, 2799 (2002).
- [19] D. S. G. Bauer, “Development of a relativistic full-potential first-principles multiple scattering Green function method applied to complex magnetic textures of nanostructures at surfaces,” *Forschungszentrum Jülich* (2014).
- [20] J. P. Perdew, K. Burke, and M. Ernzerhof, “Generalized gradient approximation made simple,” *Phys. Rev. Lett.* **77**, 3865–3868 (1996).
- [21] A. I. Liechtenstein, M. I. Katsnelson, and V. A. Gubanov, “Exchange interactions and spin-wave stiffness in ferromagnetic metals,” *Journal of Physics F: Metal Physics* **14**, L125 (1984).
- [22] H. Ebert and S. Mankovsky, “Anisotropic exchange coupling in diluted magnetic semiconductors: Ab initio spin-density functional theory,” *Phys. Rev. B* **79**, 045209 (2009).
- [23] I. V. Solovyev, “Exchange interactions and magnetic force theorem,” *Phys. Rev. B* **103**, 104428 (2021).
- [24] E. Mendive-Tapia, M. dos Santos Dias, S. Grytsiuk, J. B. Staunton, S. Blügel, and S. Lounis, “Short period magnetization texture of B20-MnGe explained by thermally fluctuating local moments,” *Phys. Rev. B* **103**, 024410 (2021).
- [25] See Supplemental Material, which contains references [42–46], for further details on the Fourier transform of the magnetic interactions and the construction of the magnetic phase diagram. We also show additional plots for Fermi surface cuts of Gd₂PdSi₃, the density of states of the two materials studied, components of spin structure factors, and a list of material families which may host skyrmions.
- [26] J. Bouaziz, M. d. S. Dias, A. Ziane, M. Benakki, S. Blügel, and S. Lounis, “Chiral magnetism of magnetic adatoms generated by rashba electrons,” *New Journal of Physics* **19**, 023010 (2017).
- [27] H. Ebert, D. Koedderitzsch, and J. Minar, “Calculating condensed matter properties using the KKR-Green’s function method—recent developments and applications,” *Reports on Progress in Physics* **74**, 096501 (2011).
- [28] A. J. Pindor, J. Staunton, G. M. Stocks, and H. Winter, “Disordered local moment state of magnetic transition metals: a self-consistent KKR CPA calculation,” *Journal of Physics F: Metal Physics* **13**, 979 (1983).
- [29] J. Staunton, B. L. Gyorffy, A. J. Pindor, G. M. Stocks, and H. Winter, “The “disordered local moment” picture of itinerant magnetism at finite temperatures,” *Journal of magnetism and magnetic materials* **45**, 15–22 (1984).
- [30] B. L. Gyorffy, A. J. Pindor, J. Staunton, G. M. Stocks, and H. Winter, “A first-principles theory of ferromagnetic phase transitions in metals,” *Journal of Physics F: Metal Physics* **15**, 1337 (1985).
- [31] D. S. Inosov, D. V. Evtushinsky, A. Koitzsch, V. B. Zabolotnyy, S. V. Borisenko, A. A. Kordyuk, M. Frontzek, M. Loewenhaupt, W. Löser, I. Mazilu, H. Bitterlich, G. Behr, J.-U. Hoffmann, R. Follath, and B. Büchner, “Electronic structure and nesting-driven enhancement of the rky interaction at the magnetic ordering propagation vector in gd₂pdsi₃ and tb₂pdsi₃,” *Phys. Rev. Lett.* **102**, 046401 (2009).
- [32] A. Devishvili, *Magnetic properties of Gd3+ based systems*, Ph.D. thesis, uniwiien (2010).
- [33] A. Garnier, D. Gignoux, N. Iwata, D. Schmitt, T. Shigeoka, and F. Y. Zhang, “Anisotropic metamagnetism in GdRu₂Si₂,” *Journal of magnetism and magnetic materials* **140**, 899–900 (1995).
- [34] F. N. Rybakov, N. S. Kiselev, A. B. Borisov, L. Döring, C. Melcher, and S. Blügel, “Magnetic hopfions in solids,” *arXiv preprint arXiv:1904.00250* (2019).
- [35] Sergii Grytsiuk, J-P Hanke, Markus Hoffmann, Juba Bouaziz, Olena Gomonay, Gustav Bihlmayer, Samir Lounis, Yuriy Mokrousov, and Stefan Blügel, “Topological-chiral magnetic interactions driven by emergent orbital magnetism,” *Nature communications* **11**, 1–7 (2020).
- [36] G. P. Müller, M. Hoffmann, C. Dißelkamp, D. Schürhoff, S. Mavros, M. Sallermann, N. S. Kiselev, H. Jónsson, and S. Blügel, “Spirit: Multifunctional framework for atomistic spin simulations,” *Phys. Rev. B* **99**, 224414 (2019).
- [37] M. Hoffmann, B. Zimmermann, G. P. Müller, D. Schürhoff, N. S. Kiselev, C. Melcher, and S. Blügel, “Antiskyrmions stabilized at interfaces by anisotropic dzyaloshinskii-moriya interactions,” *Nature communications* **8**, 1–9 (2017).
- [38] A. O. Leonov and M. Mostovoy, “Multiply periodic states and isolated skyrmions in an anisotropic frustrated magnet,” *Nature communications* **6**, 1–8 (2015).
- [39] S. Spachmann, A. Elghandour, M. Frontzek, W. Löser, and R. Klingeler, “Magnetoelastic coupling and phases in the skyrmion lattice magnet Gd₂PdSi₃ discovered by high-resolution dilatometry,” *Phys. Rev. B* **103**, 184424 (2021).
- [40] Zhipeng Hou, Lingwei Li, Chen Liu, Xingsen Gao, Zhipan Ma, Guofu Zhou, Yong Peng, Mi Yan, Xi-xiang Zhang, and Junming Liu, “Emergence of room temperature stable skyrmionic bubbles in the rare earth based REMn₂Ge₂ (RE= Ce, Pr, and Nd) magnets,” *Materials Today Physics* **17**, 100341 (2021).
- [41] Christoph J Raub, “Handbook of magnetic materials, volume 6: edited by khj buschow, isbn 0-444-88952-3, us 214, 654 pp., more than 500 illustrations,” (1993).
- [42] E. Mendive-Tapia and J. B. Staunton, “Ab initio theory of the Gibbs free energy and a hierarchy of local moment correlation functions in itinerant electron systems: The magnetism of the Mn₃A materials class,” *Phys. Rev. B* **99**, 144424 (2019).
- [43] R. Elliott, *Magnetic properties of rare earth metals* (Springer Science & Business Media, 2013).
- [44] B. L. Gyorffy, “Coherent-Potential Approximation for a nonoverlapping-muffin-tin-potential model of random substitutional alloys,” *Phys. Rev. B* **5**, 2382–2384 (1972).
- [45] P. Soven, “Coherent-potential model of substitutional disordered alloys,” *Phys. Rev.* **156**, 809–813 (1967).
- [46] S. Hayami and R. Yambe, “Meron-antimeron crystals in noncentrosymmetric itinerant magnets on a triangular lattice,” *Phys. Rev. B* **104**, 094425 (2021).